SOIL CARBON

Size, distribution, and vulnerability of the global soil inorganic carbon

Yuanyuan Huang[1,2]†*, Xiaodong Song[3]†, Ying-Ping Wang[4], Josep G. Canadell[5], Yiqi Luo[6], Philippe Ciais[7], Anping Chen[8], Songbai Hong[9], Yugang Wang[10], Feng Tao[11], Wei Li[12], Yiming Xu[13], Reza Mirzaeitalarposhti[14], Heba Elbasiouny[15], Igor Savin[16,17], Dmitry Shchepashchenko[18,19,20], Raphael A. Viscarra Rossel[21], Daniel S. Goll[7], Jinfeng Chang[18,22], Benjamin Z. Houlton[11], Huayong Wu[3], Fei Yang[3], Xiaoming Feng[23], Yongzhe Chen[24], Yu Liu[1], Shuli Niu[1], Gan-Lin Zhang[3,25,26]*

Global estimates of the size, distribution, and vulnerability of soil inorganic carbon (SIC) remain largely unquantified. By compiling 223,593 field-based measurements and developing machine-learning models, we report that global soils store 2305 ± 636 (±1 SD) billion tonnes of carbon as SIC over the top 2-meter depth. Under future scenarios, soil acidification associated with nitrogen additions to terrestrial ecosystems will reduce global SIC (0.3 meters) up to 23 billion tonnes of carbon over the next 30 years, with India and China being the most affected. Our synthesis of present-day land-water carbon inventories and inland-water carbonate chemistry reveals that at least 1.13 ± 0.33 billion tonnes of inorganic carbon is lost to inland-waters through soils annually, resulting in large but overlooked impacts on atmospheric and hydrospheric carbon dynamics.

Soil inorganic carbon (SIC) (supplementary materials, soil carbonate system) is conventionally viewed as a relatively stable carbon pool with an assumed turnover time of millennia (*1*, *2*). This view is shifting as evidence of accelerated SIC dynamics is growing, revealing substantial perturbations to SIC within several decades (*3*–*5*), an increasing trend of alkalinity in major rivers worldwide (*6*–*8*), and stores of soil-sourced new bicarbonate ions in groundwaters (*5*, *9*, *10*). The altered SIC, in turn, is impacting the acidity-buffering capacity, nutrient availability, plant productivity, and organic carbon stabilization of terrestrial soils (*11*–*15*), highlighting the role of SIC not only in carbon sequestration, but also for soil health, ecosystem services, and ecosystem functions (*16*).

Solid SIC consists of lithogenic, biogenic, and pedogenic carbonates (*17*). Pedogenic carbonate is typically formed through dissolution of solid minerals to cations, which reprecipitate with dissolved inorganic carbon (DIC) as carbonate minerals in soil, regulated by hydrology and soil microenvironments that modulate the equilibrium reactions of the carbonate system (eqs. S1 and S2) (*17*, *18*). Water movement partly reprecipitates SIC into deep soils and partly removes DIC (therefore, solid SIC) from soils through drainage, which mediates carbon dynamics in fresh and ocean waters. SIC links organic-inorganic processes in the carbon cycle and connects land–water (ocean)–atmosphere across timescales from fast carbonate kinetics within hours to Earth's geological history. Unfortunately, it is typically not included in carbon budgeting (*19*), leaving its size, distribution, influencing factors, and fate largely unknown. Bridging these gaps and disentangling the role of SIC in the global carbon cycle is urgent considering the rapid rates of carbonate reactions, the enormous global SIC stock [from 695 to 940 billion tonnes of carbon (GtC) in the top 1 m of soil to >1000 GtC in the top 2 m of soil; table S1) (*1*, *2*, *20*–*23*), its huge impacts on hydrospheric carbon geochemistry, and the fact that a small change of that stock may have large impacts on atmospheric CO_2 concentration and therefore global warming.

Quantifying global SIC storage

In this work, we collated a global SIC database with 223,593 measurements of 55,077 soil profiles from an extensive compilation of field measurements of SIC content from site studies, country-level inventories, coordinated field campaigns and standardized global soil databases (supplementary text 1) (figs. S1 and S2). This database includes samples from all 12 United States Department of Agriculture soil orders, almost every continent, climate zone, and biome across the globe (Fig. 1) and provides insights into the global pattern of SIC. The SIC content is highly variable (from 0 to >100 g(C) kg^{-1} soil) (top 2 m, Fig. 1, A and C), with 42% of the samples having a SIC value of 0 g(C) kg^{-1} (Fig. 1). The SIC-bearing (SIC > 0) soil samples worldwide show that the mean SIC content generally increases with soil depth (top 2 m, Fig. 1B) and is higher for samples with stronger alkalinity (pH > 9 versus pH between 7 and 9), whereas acidic soils are generally depleted in SIC (pH < 5, Fig. 1D). However, SIC content is also found to vary greatly among soils with the same pH (fig. S3).

We developed machine learning models that link measured SIC content to spatially explicit data on climate, topography, lithology, vegetation, soil properties, and anthropogenic activities (table S2). We used the models to make inferences on the global distribution of SIC through integrating knowledge of the source, formation, transportation, and persistence of SIC with advancements in observations, theories, and computations (materials and methods). To avoid the bias toward zero with one-step statistical models, we first trained a classification model (materials and methods for covariates) to predict whether the soil (particle size ≤2mm) is depleted of SIC (SIC = 0 or not) and then used a regression model to quantify the amount of SIC where it is >0. On the basis of established data-driven relationships, the classification and regression models [classification: area under curve (AUC) = 0.99, F score = 0.95;

[1]Key Laboratory of Ecosystem Network Observation and Modeling, Institute of Geographic Sciences and Natural Resources Research, Chinese Academy of Sciences, Beijing 100101, China. [2]State Key Laboratory of Resources and Environmental Information System, Institute of Geographic Sciences and Natural Resources Research, Chinese Academy of Sciences, Beijing 100101, China. [3]State Key Laboratory of Soil and Sustainable Agriculture, Institute of Soil Science, Chinese Academy of Sciences, Nanjing 210008, China. [4]CSIRO Environment, Private Bag 10, Clayton South VIC 3169, Australia. [5]CSIRO Environment, Black Mountain, ACT 2601, Australia. [6]Soil and Crop Sciences Section, School of Integrative Plant Science, Cornell University, Ithaca NY 14853, USA. [7]Laboratoire des Sciences du Climat et de l'Environnement, CEA/CNRS/UVSQ/Université Paris Saclay, Gif-sur-Yvette 91990, France. [8]Department of Biology and Graduate Degree Program in Ecology, Colorado State University, Fort Collins, CO 80523, USA. [9]School of Urban Planning and Design, Shenzhen Graduate School, Peking University, Shenzhen 518055, China. [10]State Key Laboratory of Desert and Oasis Ecology, Xinjiang Institute of Ecology and Geography, Chinese Academy of Sciences, Urumqi, Xinjiang 830011, China. [11]Department of Ecology and Evolutionary Biology and Department of Global Development, Cornell University, Ithaca, New York 14853, USA. [12]Department of Earth System Science, Ministry of Education Key Laboratory for Earth System Modelling, Institute for Global Change Studies, Tsinghua University, Beijing 100084, China. [13]School of Grassland Science, Beijing Forestry University, Beijing 100083, China. [14]Institute of Crop Science (340i), University of Hohenheim, Fruwirthstraße 20, 70599 Stuttgart, Germany. [15]Agriculture Faculty (Girls), Al-Azhar University, Cairo 11651, Egypt. [16]V.V. Dokuchaev Soil Science Institute, Moscow 119017, Russia. [17]Institute of Environmental Engineering of RUDN University, Moscow 117198, Russia. [18]International Institute for Applied Systems Analysis (IIASA) Schlossplatz 1, 2361 Laxenburg, Austria. [19]Center for Forest Ecology and Productivity of the Russian Academy of Sciences, Moscow 117997, Russia. [20]Institute of Ecology and Geography, Siberian Federal University, 79 Svobodny Prospect, 660041 Krasnoyarsk, Russia. [21]Soil and Landscape Science School of Molecular and Life Sciences, Faculty of Science and Engineering, Curtin University, GPO Box U1987, Perth WA 6845, Australia. [22]College of Environmental and Resource Sciences, Zhejiang University, Hangzhou 310058, China. [23]Research Center for Eco-Environmental Sciences, Chinese Academy of Sciences, Beijing 100085, China. [24]Department of Geography, The University of Hong Kong, Hong Kong 999077, China. [25]College of Advanced Agronomy, University of Chinese Academy of Sciences, Beijing 100049, China. [26]Nanjing Institute of Geography and Limnology, Chinese Academy of Sciences, Nanjing 210008, China.
*Corresponding author. Email: yuanyuanhuang2011@gmail.com (Y.H.); glzhang@issas.ac.cn (G.-L.Z.)
†These authors contributed equally to this work.

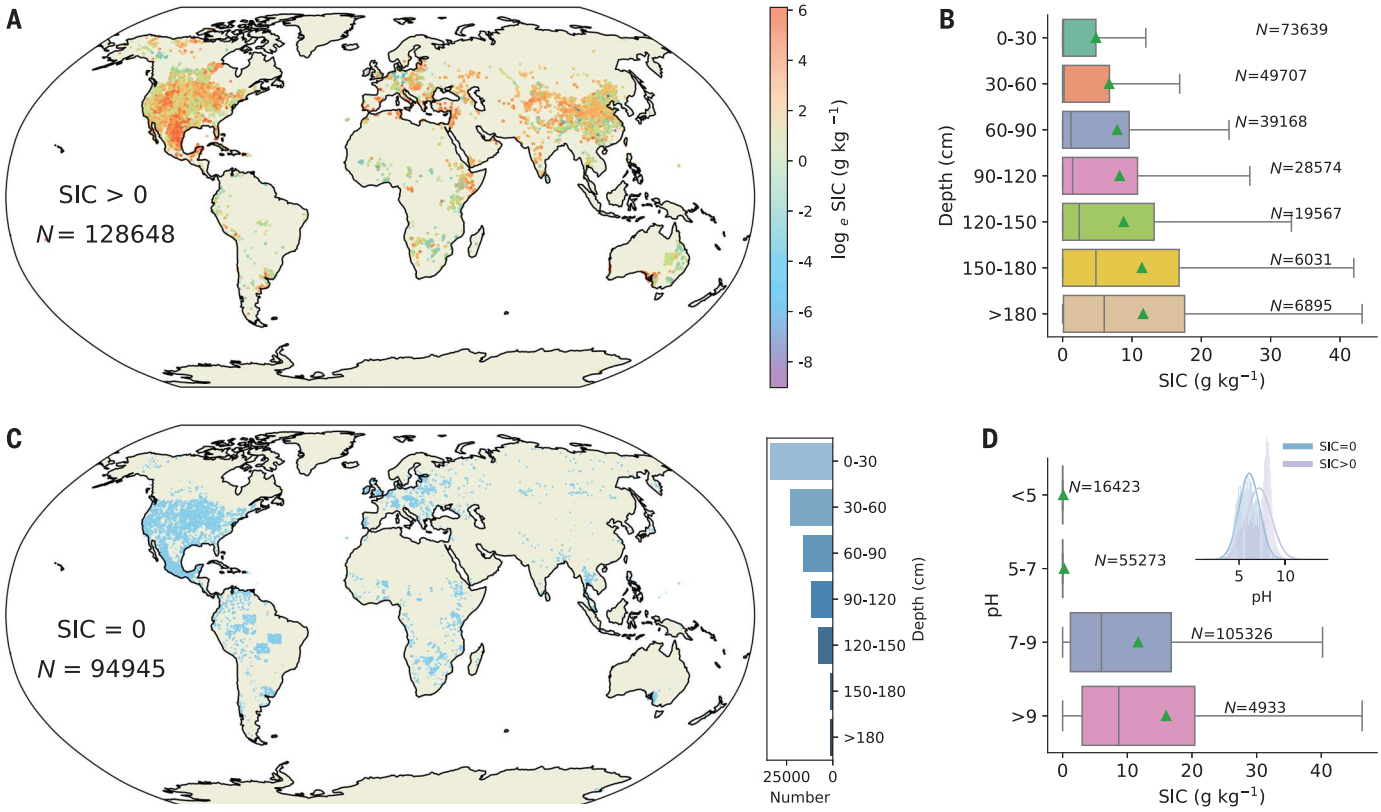

Fig. 1. Distribution of raw observations of SIC content. Spatial distribution of sample locations for (**A**) SIC > 0 and (**C**) SIC = 0. Note that samples from different depths are shown, and the size of the dots is arbitrary. (**B**) The median, mean (green triangle), and interquartile range of SIC contents for samples with SIC > 0 along the vertical soil profile. (**D**) The median, mean (green triangle), and interquartile range of SIC contents for all samples binned by soil pH classes. The inset in (C) shows the sample size (SIC = 0) in different soil depths, and the inset in (D) shows the distribution of soil pH for samples with SIC = 0 (blue) and SIC > 0 (purple).

regression: R^2 = 0.79, root mean square error = 6.17 g kg^{-1}, 10-fold cross-validation (materials and methods)] (Fig. 2, D and E, and table S3) provide a spatially explicit estimation of global SIC at a 30–arc sec resolution (~1-km^2 at the equator) (Fig. 2 and figs. S4 to S6) to a depth of 2 m and quantitative insights into influences on SIC storage. Compared with earlier land or soil unit-based methods, our estimation method captures more heterogeneity and variations in real-world SIC (supplementary text 2 and table S4). This improvement was achieved by intricately linking SIC to the local environment through multiple environmental covariates and was further strengthened by the large database measuring SIC.

Present-day (roughly 1980 to present) global total SIC is 2305 ± 636 (±1 SD) GtC in the top 2 m of soil (supplementary text 2 and tables S1, S4, and S5). High SIC content [>50 kg (C) m^{-2}] occurs in arid regions (e.g., Middle East, African Sahara, and Midwest US) (Figs. 1 and 2 and fig. S7). High SIC is also found in cold and temperate humid zones, especially along rivers, lakes, and coastal areas with calcium-rich alluvial deposits or calcareous parent material (figs. S7 and S8). Locally, geological background and aeolian processes have strong influence on SIC content. Karst region soils typically contain lithological carbonate, whereas in areas such as central Asia, loess deposition contributes to a high content of carbonate minerals. Low water availability associated with low precipitation and high evapotranspiration in arid, semiarid, and subhumid regions (fig. S7) limits the dissolution and leaching of carbonates from soils. These regions account for roughly 80% of the global SIC stock (table S6) within less than half of the global land area. Humid regions contain 17% of the global SIC in the topsoil (0 to 0.3 m), but their relative contribution increases with soil depth [18%, 0.3 to 1 m; 20%, 1 to 2 m (table S6)]. By soil types, Aridisols and Entisols hold around half of the global total SIC (~1150 GtC), whereas Inceptisols, Mollisols, Gelisols, Alfisols and Vertisols store 276, 274, 238, 139, and 62 GtC SIC, respectively (fig. S9 and table S7). By country, Russia, owing to its vast land area and deeper soil SIC accumulation (supplementary text 2 and fig. S10), ranks first in total SIC (0 to 2 m of soil), followed by the United States, China, Canada, Australia, Saudi Arabia, Kazakhstan, Iran, Algeria, and Argentina (table S8).

Covariates explain the global SIC distribution

The size and distribution of SIC are contingent on complex interactions among soil parent materials, edaphic conditions, biology, climate, topography, and anthropogenic impacts (Fig. 3 and supplementary text 3). Soil pH emerged as the most important predictor for the presence of SIC (contribution to modeled variations: pH, 29%; temperature annual range, 4.9%; temperature seasonality, 3.0%; cation exchange capacity, 2.6%; precipitation of the coldest quarter, 2.3%; soil silt content, 2.3%), revealed by the Shapley values that quantify the average marginal contributions of corresponding predictors based on the cooperative game theory (*24*), and its influence was confounded by environmental conditions. Soil pH itself is an integrative indicator that reflects the complex interactions between soil and its environment [e.g., climate conditions and water balance (*25*)]. Whereas the dissolution of carbonate minerals and, therefore, their subsequent losses depend on soil pH (eqs. S1 and S2), the occurrence of SIC, in turn, acts as a buffer in regulating soil pH.

Whereas the links between the kinetics of the carbonate system and pH are well established in freshwater and ocean water (eqs. S1 and S2),

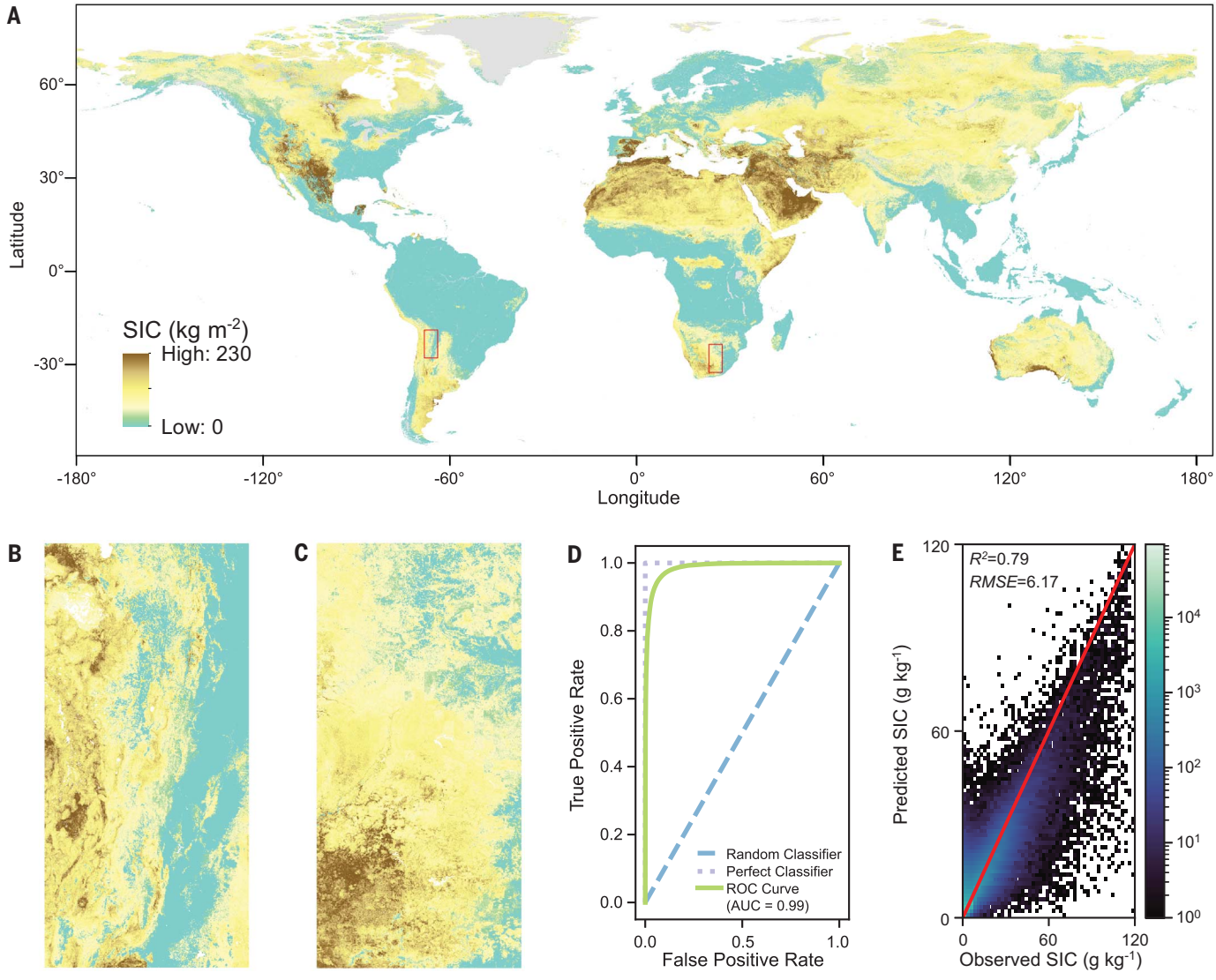

Fig. 2. The global map of SIC of the top 2 m of soil at the 1-km^2 spatial resolution. (**A**) The global distribution of SIC. (**B** and **C**) Illustration of details through examples of (B) South America and (C) Africa [red rectangles in (A)]. The map was generated through two steps: first with a classifier (N = 223,593) to predict whether SIC is zero and then with a regression model to predict the magnitude of SIC (N = 128,648) for nonzero samples. (**D**) Receiver operating characteristic (ROC) curve (green) shows the performance of the classification model (SIC > 0 versus SIC = 0) with 10-fold cross validation. AUC = 1 (purple dashed curve) means that the classifier is able to perfectly predict these two classes correctly. (**E**) Observed versus predicted SIC content for samples with nonzero SIC values made by using 10-fold cross validation. The red line indicates the 1:1 line, and the legend indicates the number of samples.

the relationship between SIC and soil pH is more intricate and dependent on the heterogeneous nature of soil environments (fig. S3). We disentangled the contribution of soil pH to variations (differences from the mean value) of SIC content, which we call SIC_{pH}, as the marginal effect of pH using the Shapley values (*24*) (materials and methods and supplementary Text 4).

A universal sigmoid-type function emerged from data that generalized the relationship between soil pH and SIC_{pH} ($SIC_{pH} = c + \frac{b}{a+e^{-k(pH-x0)}}$, where a, b, c, k, and $x0$ are empirical parameters). SIC changes abruptly with pH in the range of 7 to 8.5 and is less responsive to pH in acidic or strong alkaline environments (Fig. 3 and figs. S11 to S13). This pH-SIC_{pH} relationship is consistent with theoretical knowledge of the carbonate chemistry, whereas parameters of the fitted sigmoidal curve characterize soil environments that differ among soil orders, depths, and vegetation status (supplementary text 5, 6, and 7; figs. S11 to S14; and table S9). SIC in Alfisols and Mollisols showed the smallest slopes (small k) given their capability to neutralize H^+ from sources other than SIC (e.g., organic matter and clay minerals). Deep soil holds hold more SIC in strong alkaline conditions compared with the topsoil, which indicates a potentially larger SIC loss from deep soils if the soil pH undergoes an equivalent reduction (b/a; fig. S11). The emerging sigmoidal pH-SIC_{pH} relationship offers general guidance on the effectiveness of altering pH for preserving SIC. Soil pH alone only captured 12.6% of the modeled spatial variations of SIC in SIC-bearing (SIC > 0) soils, followed by cation exchange capacity (4.8%), drought severity index (3.2%), and other environmental factors (supplementary text 3).

Vulnerability of SIC to pH changes

Soil acidification has intensified SIC losses worldwide (*4*, *26*, *27*). From a sensitivity analysis, we found that a uniform 0.1- to 0.5-unit reduction of soil pH (top 0.3 m of soil) globally could release an additional 9 to 55 GtC of SIC (Fig. 4 and figs. S15 and S16). Regionally, the United

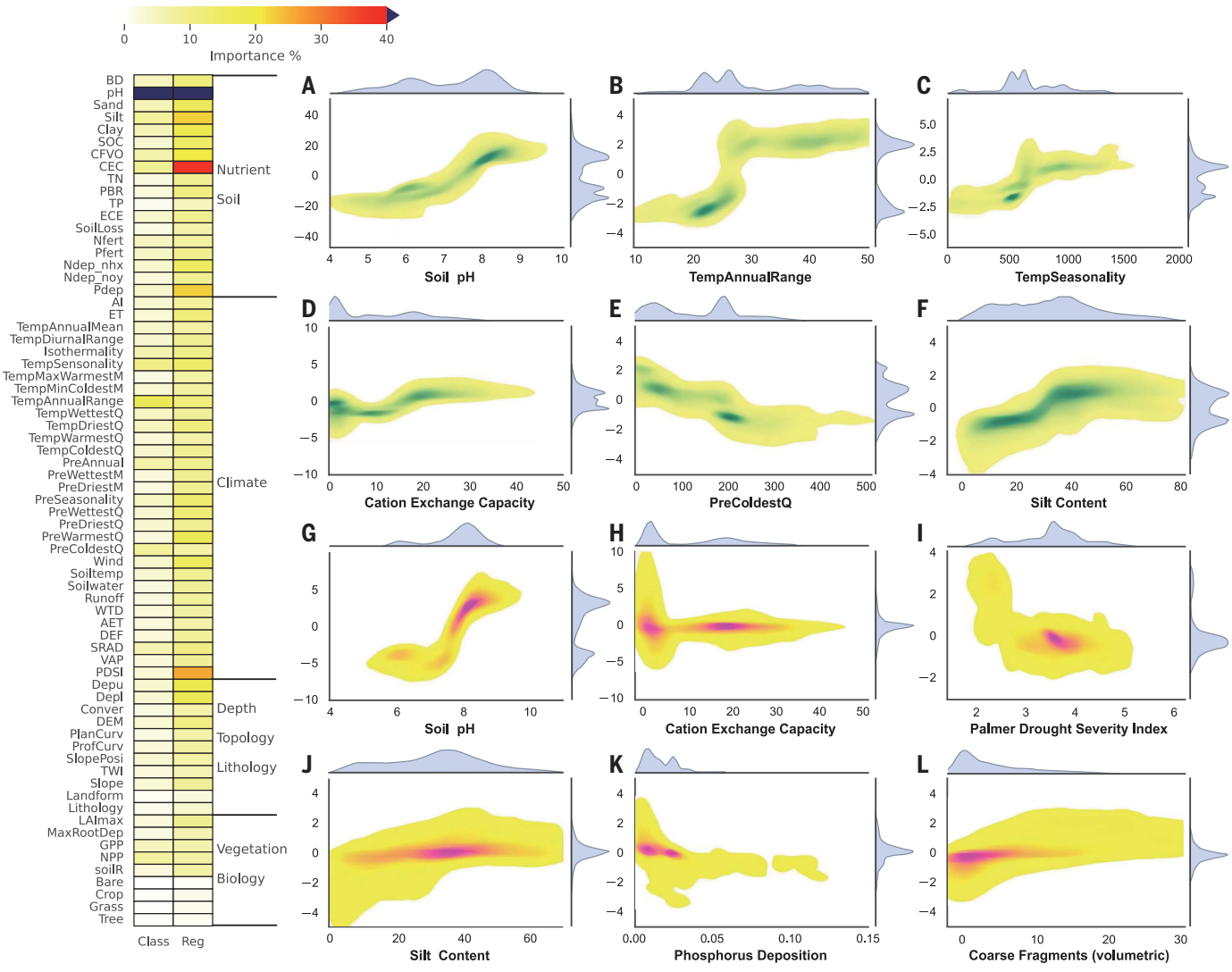

Fig. 3. Predictors of SIC. The table summarizes the relative importance (in reference to the most important predictor, i.e., pH) of each predictor in predicting whether SIC is zero (Class, classification; left column) and the nonzero values of SIC (Reg, regression; right column). (**A** to **L**) The responses of Shapley values to the top six most important predictors for classification (green) and regression (pink). Panels are shown as joint plots in which the colors in the main plot indicate the density of samples (high density, green or pink), with marginal plots showing the distributions of predictor (top) and response (right). A description of the predictors and their long names is provided in table S2.

States ranks first in terms of the sensitivity of SIC reductions to acidification, followed by Australia, Argentina, Russia, and Mexico (Fig. 4). Realistically, the magnitude of acidification varies across regions. Among different natural processes and anthropogenic factors that contribute to soil pH changes, we focused on two of the most important contributors: climate change and nitrogen additions.

Future global warming and its alteration of the hydrological cycle–induced soil pH changes (fig. S17) will result in the reduction of SIC (top 0.3 m of soil) by 1.35, 3.45, and 5.83 GtC under around 1.8°C (shared socioeconomic pathway model SSP1-2.6, sustainable development with low greenhouse gas emission) (*28*), 2.7°C (SSP2-4.5, middle-of-the-road socioeconomic development with intermediate emission), and 4.4°C warming (SSP5-8.5, fossil-fueled socioeconomic development without climate mitigation efforts with high emission) by the year 2100, respectively. By country, Saudi Arabia, India, Australia, Sudan, and Chad would experience the largest SIC losses (2.69, 1.56, 0.89, 0.76, and 0.64 GtC, respectively) under 4.4°C warming, whereas Russia, the United States, Spain, France, and Kazakhstan would have the highest increases in SIC [0.74, 0.73, 0.62, 0.44, and 0.40 GtC, respectively (table S10)], partly owing to regional variations in the sensitivity to soil pH and future climate-driven changes in soil pH (materials and methods). Over croplands, we found that 0.43, 0.35, and 0.18 GtC of SIC losses occurred globally under SSP1-2.6, SSP2-4.5, and SSP5-8.5, respectively. The lower net SIC losses observed under a warmer future are due to a greater number of locations experiencing relatively larger gains and losses, effectively offsetting each other on a global scale. These findings offer quantitative evidence supporting the more pronounced disturbances to SIC (locally or globally) in the face of a warmer future climate. This emphasizes the imperative for climate policies to prioritize substantial reductions in greenhouse gas emissions, thereby mitigating the potential for increased disruptions to SIC.

Combining a field-established quantitative relationship that relates changes in soil pH to cumulative nitrogen fertilizer inputs, future nitrogen policy scenarios, and our SIC models

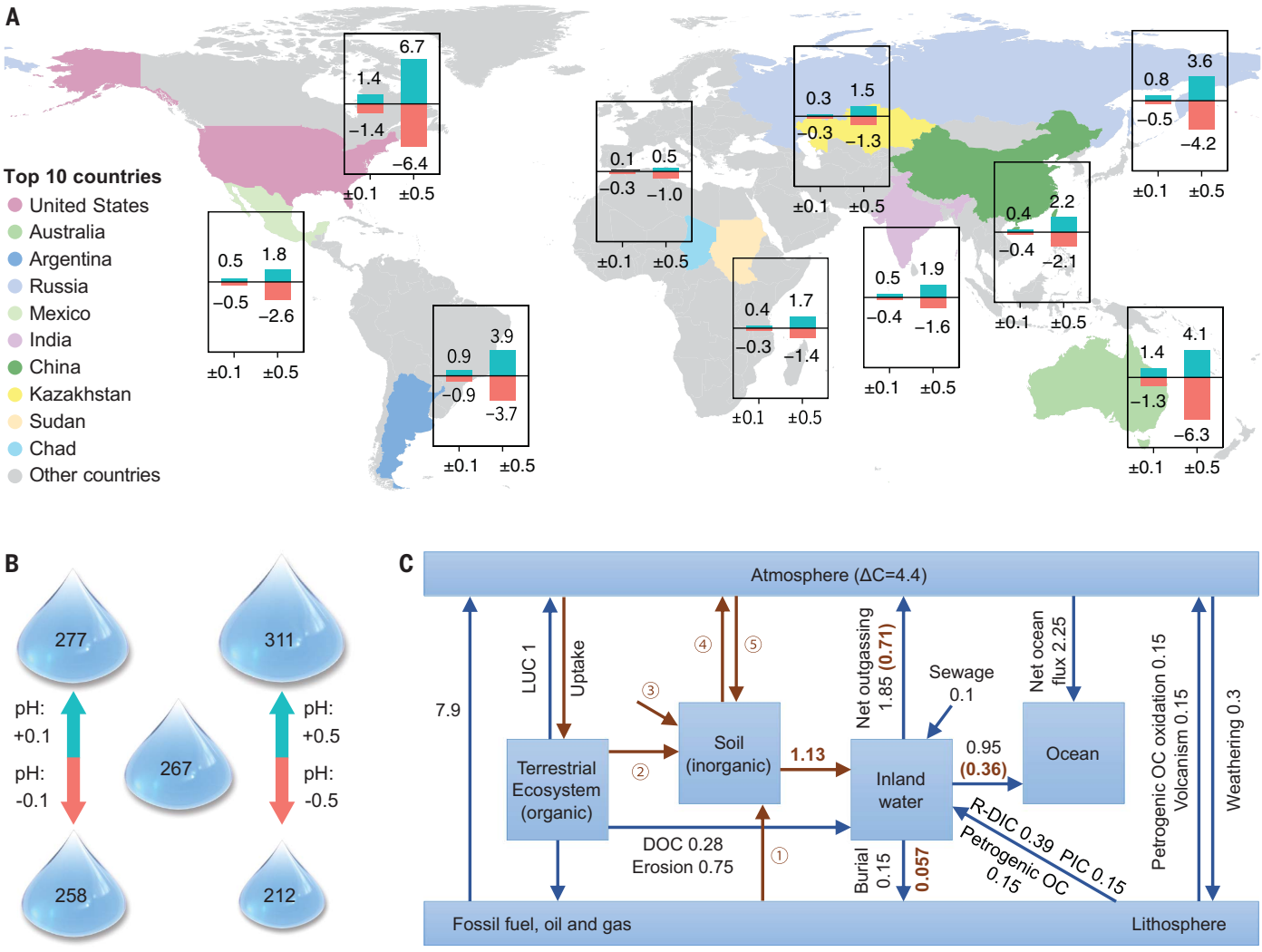

Fig. 4. SIC-relevant global budgets. (**A**) Changes in SIC (top 0.3 m) in response to soil pH by countries. Cyan bars (in units of GtC) indicate the gain of SIC in response to a higher pH (by two levels: 0.1 and 0.5), whereas red bars show the loss in response to acidification. We show the top 10 countries ranked by SIC losses (pH reduction by 0.1) from high to low. (**B**) Global SIC stock (top 0.3 m, in units of GtC) in response to soil pH. (**C**) Flowchart of the present-day global carbon budget (in units of GtC yr^{-1}) accounting for inorganic carbon exchanges through soil (materials and methods and fig. S19). Fluxes that have been altered owing to the inclusion of inorganic carbon through soils are in brown, whereas fluxes in blue arrows are adapted from references (*37*, *47*–*50*). In brackets are the contributions of SIC to total fluxes (in the case of more than one contributing sources). We used Terrestrial Ecosystem to refer to land that excludes inland waters. DOC, dissolved organic carbon export from leaching and runoff; R-DIC, lateral inorganic carbon export from bedrock weathering; PIC, physical erosion of total recalcitrant particulate inorganic carbon; petrogenic OC, organic carbon export from fossil and old soil; erosion, lateral organic carbon export from water, wind, and tillage erosions. Pathway 1 represents the inorganic carbon flux from rock to soil, and its contribution to inland-water is accounted through R-DIC; pathway 2 represents SIC fluxes sourced from terrestrial biological system (e.g., respiration); pathway 3 is external inorganic carbon inputs into soils (e.g., lime); and pathways 4 and 5 are carbon exchanges between SIC and the atmosphere.

(materials and methods), we estimate that nitrogen addition–induced (nitrogen deposition plus fertilization) acidification over the next 30 years (2020 to 2050) will reduce the topsoil SIC by 10, 14, and 23 GtC under SSP1-2.6-High-Ambition-N (i.e., with a low level of mineral nitrogen inputs), SSP2-4.5-Medium-Ambition-N (i.e., with a medium level of mineral nitrogen inputs), and SSP5-8.5-Low-Ambition-N policy scenarios (i.e., with a high level of mineral nitrogen inputs), respectively. The most substantial changes under the SSP5-8.5-Low-Ambition-N scenario highlight the large disturbance of nitrogen fertilizations on the terrestrial inorganic carbon cycle. The highest SIC losses will come from India and China (SSP5-8.5-Low-Ambition-N) owing to rapid soil acidification in croplands (fig. S18 and table S11).

Discussion

The large SIC pool and its high vulnerability to acidification-induced losses may pose a risk to limiting net CO_2 emissions to the atmosphere to be consistent with the temperature targets of the Paris Agreement (*26*, *27*). Determining whether losses of SIC act as a sink or source of atmospheric CO_2 at the decadal scale is complex, contingent on spatial scales and the examined components of the Earth system (*3*, *9*, *29*–*32*). There are three major fates of the lost solid SIC: dissolution-reprecipitation in deeper soils, export to the hydrosphere through DIC, and degassing (SIC dissolution generates CO_2 instead of HCO_3^- under very strong acidity). Dissolution-reprecipitation does not contribute to net soil carbon exchanges (*18*, *29*). By combining two approaches derived from the comprehensive land-water carbon inventories and inland water carbonate chemistry

based on existing studies, we estimate that at least 1.13 ± 0.33 (± 1 SD) Gt of inorganic carbon is transported through soils to inland waters (f_{SIC2W}) each year that cannot be explained by rock weathering (materials and methods) (Fig. 4C and fig. S19). This carbon might be sourced from organic matter decomposition and root respiration (*33*) (nonsolid SIC), lime applied to soils (*30*, *31*, *34*), and in situ solid SIC (*3*, *5*, *35*) and might enter surface water or ground water (*10*, *30*, *34*, *36*). Despite the mixed carbon sources, our study emphasizes the importance of the often-overlooked inorganic pathway through soils in the present-day carbon dynamics (*10*, *18*, *27*, *36*), especially as one of the primary pathways of land-aquatic carbon exchange (Fig. 4).

As a thought experiment, we assume that all f_{SIC2W} are sourced from solid SIC, in which case, the dissolution of carbonate to produce and export DIC (mainly HCO_3^-) would result in the uptake of 0.56 GtC yr^{-1} of CO_2 from the atmosphere. The portion of SIC dissolved by strong acids that leads to releasing of CO_2 ranges from 12 to 38% from European and North American watersheds (*30*, *31*, *34*, *35*). Based on a rough estimate with a median global value of 25%, the degassing flux is expected to release 0.19 GtC yr^{-1} (materials and methods) to the atmosphere. Losses of soil-mediated inorganic carbon are, therefore, likely associated with a net uptake of 0.37 GtC yr^{-1} of the atmospheric CO_2 through global soils. The actual value of this is contingent upon the proportion of f_{SIC2W} that can be attributed to solid carbonates. Using a simple proportional scaling approach based on the recent inland-water carbon budget reported in (*37*), we estimate that after the lost carbon enters inland waters and is transported through water networks, roughly 0.71 GtC yr^{-1} is released from inland waters to the atmosphere, 0.057 GtC yr^{-1} is buried in inland waters, and 0.36 GtC yr^{-1} contributes to oceanic carbon annually (materials and methods). When considering both soils and inland waters, losses of soil-mediated carbon likely act as a carbon source, releasing 0.34 GtC yr^{-1} to the atmosphere (Fig. 4) (materials and methods) in the present day. However, when combining land and ocean, losses of soil-mediated carbon may function as a sink for atmospheric CO_2 over time, depending on how soil-mediated DIC affects oceanic carbon; the indirect effects of soil-mediated DIC on freshwater carbon dynamics; the interactions among SIC, SOC, and vegetation under global changes; and many other unaccounted factors (*32*, *38*), highlighting large uncertainties in the current understanding of the contribution of soil-mediated inorganic carbon pathways to natural and anthropogenic carbon fluxes.

Sensitivities and feedbacks of SIC to climate warming (*39*), precipitation (*5*, *12*, *40*), rising atmospheric CO_2 (*41*), and land uses (*42*) are different from the biological responses to the same drivers and therefore could alter the existing understanding of the terrestrial carbon-concentration and carbon-climate feedbacks. In addition, to some extent, the efficacy of carbon sequestration strategies, such as enhanced rock weathering, afforestation, and soil organic carbon stabilization, depends upon SIC, which affects soil and plant, such as through nutrient availability, aggregate stability, organo-mineral interactions, and water availability (*11*–*15*, *17*, *43*). Interconnections of SIC with the atmosphere, biosphere, hydrosphere, and lithosphere emphasize the interweaved role of SIC in the global carbon cycle and highlight its overlooked influence. Although estimating SIC-mediated carbon fluxes at decadal-to-century timescales involves uncertainties, our results suggest that assuming that the SIC has remained inert and unchanged since preindustrial times, as implicitly assumed by the Intergovernmental Panel on Climate Change (IPCC) (*44*) and the Global Carbon Project (GCP) (*19*) reports, requires revision. A more nuanced approach is necessary to fully understand the role of SIC in the carbon cycle.

The global map of SIC content can facilitate ongoing efforts to understand the biogeochemical cycle of inorganic carbon; monitor its changes; pinpoint places with high risk of losses; identify key influencing factors; assess human influence; and support local, national, and international carbon remediation and sequestration efforts. For example, the effectiveness of controlling pH for preserving SIC varies across regions (figs. S15 and S16), and the spatial information of SIC content could be used to limit disturbances by agriculture practices (e.g., effective nitrogen fertilization or appropriate irrigation) on SIC (*45*).

Several recent reviews (*17*, *27*, *41*, *46*) have synthesized the sources and drivers of soil acidification, the mechanisms of pedogenic carbonate formation, and the multiple factors and pathways that regulate SIC dynamics across a wide range of conditions. Results in this study provide knowledge and quantitative insights into inorganic carbon dynamics. The roadmap for achieving a comprehensive understanding of the direct and indirect roles of SIC in the present-day global carbon cycle should consider several critical and unresolved issues, including: (i) the source of cation (e.g., Ca^{2+}) to understand whether the formation of SIC contributes to sequestration of atmospheric carbon dioxide (e.g., from silicate minerals); (ii) the status of SIC below 2-m soil depth to quantify more completely the total SIC in terrestrial ecosystems worldwide; (iii) the origin of SIC (lithogenic, biogenic, and pedogenic carbonates) to understand the influences of mineral composition, living organisms, environmental factors, and soil-forming processes on carbonate dynamics; (iv) the impact of SIC on other components of the carbon cycle (e.g., SOC in terrestrial and blue carbon ecosystems and oceanic carbon); (v) the specific impacts of different management practices on SIC (e.g., liming); and (vi) the natural and anthropogenic contributions of SIC to the contemporary global carbon cycle. Disrupting the global SIC stock that has accumulated over millennia is likely to have profound impacts not only on carbon sequestration, but also on other soil processes and the Earth system (*9*, *11*, *12*, *15*, *32*).

REFERENCES AND NOTES

1. W. H. Schlesinger, *Geochim. Cosmochim. Acta* **49**, 57–66 (1985).
2. W. H. Schlesinger, *Soil Sci.* **133**, 247–255 (1982).
3. J. H. Kim, E. G. Jobbágy, D. D. Richter, S. E. Trumbore, R. B. Jackson, *Glob. Chang. Biol.* **26**, 5988–6002 (2020).
4. X. D. Song *et al.*, *Natl. Sci. Rev.* **9**, nwab120 (2022).
5. A. G. Lapenis *et al.*, *Global Biogeochem. Cycles* **22**, GB2010 (2008).
6. P. A. Raymond, J. J. Cole, *Science* **301**, 88–91 (2003).
7. T. W. Drake *et al.*, *Environ. Sci. Technol.* **52**, 8302–8308 (2018).
8. P. A. Raymond, S. K. Hamilton, *Limnol. Oceanogr. Lett.* **3**, 143–155 (2018).
9. Y. Li, Y. G. Wang, R. A. Houghton, L. S. Tang, *Geophys. Res. Lett.* **42**, 5880–5887 (2015).
10. M. Klaus, *Commun. Earth Environ.* **4**, 221 (2023).
11. M. C. Rowley, S. Grand, E. P. Verrecchia, *Biogeochemistry* **137**, 27–49 (2018).
12. M. C. Duniway, J. E. Herrick, H. C. Monger, *Oecologia* **163**, 215–226 (2010).
13. K. L. Page, D. E. Allen, R. C. Dalal, W. Slattery, *Soil Res.* **47**, 747–762 (2009).
14. S. Tunesi, V. Poggi, C. Gessa, *Nutr. Cycl. Agroecosyst.* **53**, 219–227 (1999).
15. F. Tao, B. Z. Houlton, *Glob. Chang. Biol.* **30**, e17132 (2024).
16. G. R. Groshans, E. A. Mikhailova, C. J. Post, M. A. Schlautman, *Geoderma* **324**, 37–46 (2018).
17. K. Zamanian, K. Pustovoytov, Y. Kuzyakov, *Earth Sci. Rev.* **157**, 1–17 (2016).
18. H. C. Monger *et al.*, *Geology* **43**, 375–378 (2015).
19. P. Friedlingstein *et al.*, *Earth Syst. Sci. Data* **14**, 1917–2005 (2022).
20. W. G. Sombroek, F. O. Nachtergaele, A. Hebel, *Ambio* **22**, 417–426 (1993).
21. N. H. Batjes, *Eur. J. Soil Sci.* **47**, 151–163 (1996).
22. R. Lal, J. M. Kimble, B. H. Stewart, H. Eswaran, in *Global climate change and pedogenic carbonates* (Lewis Publishers, 1999) pp. 15–27.
23. C. Plaza *et al.*, *Sci. Rep.* **8**, 13788 (2018).
24. S. M. Lundberg, S. I. Lee, in *31st Annual Conference on Neural Information Processing Systems (NIPS)*. (Long Beach, CA, 2017), vol. 30.
25. E. W. Slessarev *et al.*, *Nature* **540**, 567–569 (2016).
26. K. Zamanian, M. Zarebanadkouki, Y. Kuzyakov, *Glob. Chang. Biol.* **24**, 2810–2817 (2018).
27. S. Raza *et al.*, *J. Clean. Prod.* **315**, 128036 (2021).
28. B. C. O'Neill *et al.*, *Geosci. Model Dev.* **9**, 3461–3482 (2016).
29. W. H. Schlesinger, *Glob. Chang. Biol.* **23**, 25–27 (2017).
30. T. O. West, A. C. McBride, *Agric. Ecosyst. Environ.* **108**, 145–154 (2005).
31. S. K. Hamilton, A. L. Kurzman, C. Arango, L. X. Jin, G. P. Robertson, *Global Biogeochem. Cycles* **21**, GB2021 (2007).
32. R. Lal, C. Monger, L. Nave, P. Smith, *Philos. Trans. R. Soc. Lond. B Biol. Sci.* **376**, 20210084 (2021).
33. R. Lauerwald, P. Regnier, B. Guenet, P. Friedlingstein, P. Ciais, *One Earth* **3**, 226–236 (2020).
34. N. H. Oh, P. A. Raymond, *Global Biogeochem. Cycles* **20**, 2005GB002565 (2006).
35. K. Semhi, P. A. Suchet, N. Clauer, J. L. Probst, *Appl. Geochem.* **15**, 865–878 (2000).
36. T. J. Kessler, C. F. Harvey, *Geophys. Res. Lett.* **28**, 279–282 (2001).
37. P. Regnier, L. Resplandy, R. G. Najjar, P. Ciais, *Nature* **603**, 401–410 (2022).
38. A. Naorem *et al.*, *Agriculture* **12**, 1256 (2022).
39. C. H. Zhang, Y. Y. Sun, G. Y. Tang, F. Y. Liu, *Soil Sci.* **184**, 52–59 (2019).
40. G. M. Marion, W. H. Schlesinger, P. J. Fonteyn, *Soil Sci.* **139**, 468–481 (1985).

41. J. Ferdush, V. Paul, *Catena* **204**, 105434 (2021).
42. Y. G. Wang *et al*., *Land Degrad. Dev.* **30**, 1229–1242 (2019).
43. D. J. Beerling *et al*., *Nature* **583**, 242–248 (2020).
44. J. G. Canadell *et al*., *Climate Change 2021: The Physical Science Basis. Contribution of Working Group I to the Sixth Assessment Report of the Intergovernmental Panel on Climate Change*, V. Masson-Delmotte *et al*., Eds. (Cambridge Univ. Press, 2021), pp. 673–816.
45. J. Sanderman, *Agric. Ecosyst. Environ.* **155**, 70–77 (2012).
46. Z. A. Sun, F. Q. Meng, B. Zhu, *Soil Ecol. Lett.* **5**, 6–20 (2023).
47. M. Nakhavali *et al*., *Glob. Chang. Biol.* **27**, 1083–1096 (2021).
48. P. Regnier *et al*., *Nat. Geosci.* **6**, 597–607 (2013).
49. J. N. Quinton, G. Govers, K. Van Oost, R. D. Bardgett, *Nat. Geosci.* **3**, 311–314 (2010).
50. D. W. Yang, S. Kanae, T. Oki, T. Koike, K. Musiake, *Hydrol. Processes* **17**, 2913–2928 (2003).

ACKNOWLEDGMENTS

We thank the generous help of S. Quanxi on the mathematics of this study. We acknowledge the WoSIS database (https://www.isric.org/explore/wosis) for providing the publicly available soil property database used in this study and the University of Hohenheim for providing the Germany dataset applied in this study. **Funding:** This work was supported by the National Natural Science Foundation of China (31988102; Y.H. and S.N.); the Strategic Priority Research Program of the Chinese Academy of Sciences (Category B, Geographic Intelligence, no. XDB0740300); the National Natural Science Foundation of China (nos. 42322102 and 42130715; X.S. and G.Z.); the Natural Science Foundation of Jiangsu Province (no. BK20220093; X.S. and G.Z.); the Second Tibetan Plateau Scientific Expedition and Research Program (no. 2019QZKK0306-02; G.Z.); the Youth Innovation Promotion Association of the Chinese Academy of Sciences (no. 2021310; X.S.); the Ministry of Science and Highest Education of Russia (no. 075-15-2022-321; I.S.); and the Australian Research Council's Discovery Projects scheme (project DP210100420; R.A.V.R.).
Author contributions: Conceptualization: Y.H., X.S., Y.P.W., and G.-L.Z.; Methodology: Y.H., X.S., Y.-P.W., R.A.V.R., P.C., Yi.L., and F.T.; Investigation: Y.H.; Visualization: Y.H. and X.S.; Funding acquisition: Y.H., X.S., and G.-L.Z.; Project administration: Y.H.; Supervision: Y.H. and G.-L.Z.; Writing – original draft: Y.H.; Writing – review and editing: X.S., Y.-P.W., J.G.C., Yi.L., P.C., A.C., S.H., Y.W., F.T., W.L., Y.X., R.M., H.E., I.S., D.S., R.A.V.R., D.S.G., J.C., B.Z.H., H.W., F.Y., X.F., Y.C., Yu.L., S.N., and G.-L.Z. **Competing interests:** The authors declare that they have no competing interests. **Data and materials availability:** Source datasets and global maps generated in this study are available at https://figshare.com/s/26f03972cc42b2e1e09f. Calculations were conducted through python 3 and ferret/7.6.0. Data processing code and code used to generate figures are also provided through figshare at https://figshare.com/s/26f03972cc42b2e1e09f.

SUPPLEMENTARY MATERIALS

Submitted 17 May 2023; accepted 7 March 2024
10.1126/science.adi7918